



Check for updates



# Nondestructive Detection of Water Ingress in Solar Modules Using Near-Infrared Absorbance Spectroscopy

Oleksandr Mashkov 📵 | Oleksandr Stroyuk 📵 | Claudia Buerhop 🔞 | Sanna Bind | Dylan Clark | Jens Hauch 📵 | Ian Marius Peters

Helmholtz-Institut Erlangen Nürnberg für Erneuerbare Energien (HI ERN), Forschungszentrum Jülich GmbH, Erlangen, Germany

Correspondence: Oleksandr Mashkov (o.mashkov@fz-juelich.de)

Received: 30 June 2025 | Revised: 29 July 2025 | Accepted: 7 August 2025

**Funding:** the German Federal Ministry for Economic Affairs and Climate Action "dig4morE", "REMBup", Grant/Award Numbers: 03EE1090B FKZ 03EWR021F; the Helmholtz Association in the framework of the innovation platform "Solar TAP", Grant/Award Number: 714-62150-3/1

Keywords: backsheet degradation | moisture ingress | near-infrared spectroscopy | nondestructive testing | photovoltaic modules | polymer aging | water index

### **ABSTRACT**

Moisture ingress is a key factor in the degradation of photovoltaic module components. This study employs near-infrared absorption spectroscopy to nondestructively quantify water uptake in backsheets and encapsulants, using a water index derived from the 1910-1920 nm absorption band. Measurements covered short-term dynamics during rainfall, long-term outdoor monitoring, and spatial mapping. Short-term monitoring showed a 14% increase in the water index within 20 min of observations. Five months of rooftop measurements revealed strong sensitivity to humidity and temperature: the index rose by 75% as relative humidity increased from 20% to 50%, and fell by 50% as temperature rose from 0°C to 40°C. Comparative field campaigns in 2021 and 2023 showed material-specific trends: under identical conditions, polyamide and fluoropolymer-coated backsheets exhibited average water index increases of 32%, while polyvinylidene fluoride showed only a 17% increase. Changes in distribution shape indicated differing moisture resistance among materials. Gravimetric analysis confirmed material-dependent water retention. Spatial mapping and immersion tests revealed localized moisture accumulation and saturation-type sorption, with uptake rates—derived via kinetic fitting—ca. 27% higher in field-aged modules than in stored ones. These results establish near-infrared spectroscopy as a scalable and noninvasive tool for detecting moisture-related degradation in photovoltaic modules.

# 1 | Introduction

Photovoltaic (PV) modules are increasingly deployed worldwide to harness solar energy. The long-term performance and reliability of these modules are subject to various degradation mechanisms, with moisture ingress being a significant contributor to several of them. Moisture can infiltrate PV modules through diffusion, permeation, or leakage, leading to detrimental effects, such as polymer delamination and corrosion of metallic components. However, insulation resistance is primarily reduced by water vapor interacting with ionic species in the polymer matrix, facilitating charge transport and electrical leakage. Water also reduces the insulation resistance of the backsheet (BS),

potentially leading to inverter shutdowns, compromised safety, and significant energy yield losses [1-3].

The susceptibility to moisture-induced degradation varies among different BS materials. For instance, polyamide (PA) and certain multilayer fluoropolymer-coated BSs exhibit distinct degradation behaviors due to variations in polarity, diffusivity, and interlayer adhesion [4, 5]. Understanding the moisture ingress pathways and the associated degradation mechanisms is crucial for improving module design and stability as well as extending service life [6].

Traditional methods for detecting moisture ingress, such as visual inspections, wet leakage tests, and performance monitoring, often

This is an open access article under the terms of the Creative Commons Attribution License, which permits use, distribution and reproduction in any medium, provided the original work is properly cited.

© 2025 The Author(s). Solar RRL published by Wiley-VCH GmbH.

fail to detect early-stage degradation. Imaging-based techniques, such as infrared thermography, electroluminescence (EL), and ultraviolet-excited fluorescence imaging (UVF), provide surface-level insights but generally lack specificity regarding internal moisture distribution and chemical interactions within multilayer laminates. Moreover, their effectiveness may be influenced by temperature, light conditions, or the operational state of the module, and they rarely offer direct quantification of water content [7–10].

Near-infrared absorption (NIRA) spectroscopy is a well-established analytical technique [11–16] that probes overtone and combination bands of molecular vibrations, particularly O–H, C–H, and N–H stretching modes. Operating in the 780–2500 nm spectral range, NIRA has been widely applied to polymer, agricultural, petroleum, and pharmaceutical analysis for many reasons, including its unique ability to nondestructively assess moisture content and chemical composition with minimal sample preparation. When applied to PV modules, NIRA enables assessment of moisture-related changes in encapsulants and BSs and differentiation of polymer types based on spectral response. The ability to characterize chemical aging and water uptake has made NIRA a promising tool for studying degradation in multilayer film stacks. The recent development of portable NIR sensors has further expanded the potential of NIRA for field deployment and high-throughput diagnostics [17–19].

Several studies have demonstrated the viability of NIRA for evaluating aging processes in PV polymers. For example, carbonyl and water indices derived from NIR spectra have been used to track oxidation and hydrolysis in ethylene-vinyl acetate (EVA) encapsulants, correlating chemical signatures with exposure time, humidity, and UV irradiance. Moisture-related changes in polyethylene terephthalate (PET)- and PA-based BSs have also been observed through NIR spectral analysis, demonstrating the method's sensitivity to diffusion and chemical degradation in multilayer structures [6, 20–23]. These findings reinforce the potential of NIRA to support materials diagnostics in both laboratory and field contexts.

This study applies NIRA spectroscopy to detect and quantify water ingress in PV modules with different BS compositions. By correlating spectral measurements with environmental exposure and sorption behavior, we assess the capability of NIRA to provide material-specific diagnostics of moisture accumulation and degradation across different measurement regimes. The results offer insights into diffusion kinetics, aging susceptibility, and the potential for high-throughput deployment of spectroscopic tools to monitor PV installations.

## 2 | Results and Discussion

This study employs four complementary experimental approaches (Scheme 1) to investigate different aspects of water ingress dynamics in PV modules:

- 1. Short-term (ca. 0.5 h) spectral field monitoring of water ingress into a PV module during a rain event.
- 2. Long-term (ca. 5 months) continuous spectral monitoring of water content evolution in rooftop-mounted modules, as a function of relative humidity (RH) and temperature.



**SCHEME 1** | Schematic overview of water ingress investigation methods used in this study.

- Comparative spectral mapping of water content in fielded modules, using point-wise measurements on 10 modules per BS type collected during two field campaigns carried out in 2021 and 2023.
- 4. Continuous spatial mapping of water ingress in a series of modules subjected to prolonged water contact for over 30 days.

# 2.1 | Short- and Long-Time Water Uptake Monitoring in PV Module BSs via NIRA Spectroscopy

The applicability of NIRA spectroscopy for detecting water ingress in PV module BSs was evaluated by field measurements conducted at a 20 MWp solar park in Germany. NIR spectra were acquired from the BS side of PV modules before and during rainfall, with an exposure duration of approximately 30 min. During the measurement, the observer remained behind the module and shielded from the rain, while maintaining the spectral probe in the same BS position and recording spectra periodically for approximately 20 min.

As shown in Figure 1a, a progressive increase in absorbance was observed around 1910–1940 nm with longer rain exposure. This region corresponds to overtone and combination bands of O–H stretching vibrations, particularly the second overtone at 1940nm, which is specific to water and less affected by overlapping polymer signals, such as C–H vibrations [24–27].

To quantify the relative water content in the BS, a water index (WI) was defined as the ratio of the integrated absorbance of the water-related band centered at 1910–1920 nm to the PET aromatic band at 1660 nm [22]. While the definition of WI is consistent with previous work, a normalization step was additionally applied in this study to express water uptake on a 0–1 scale. This approach enables

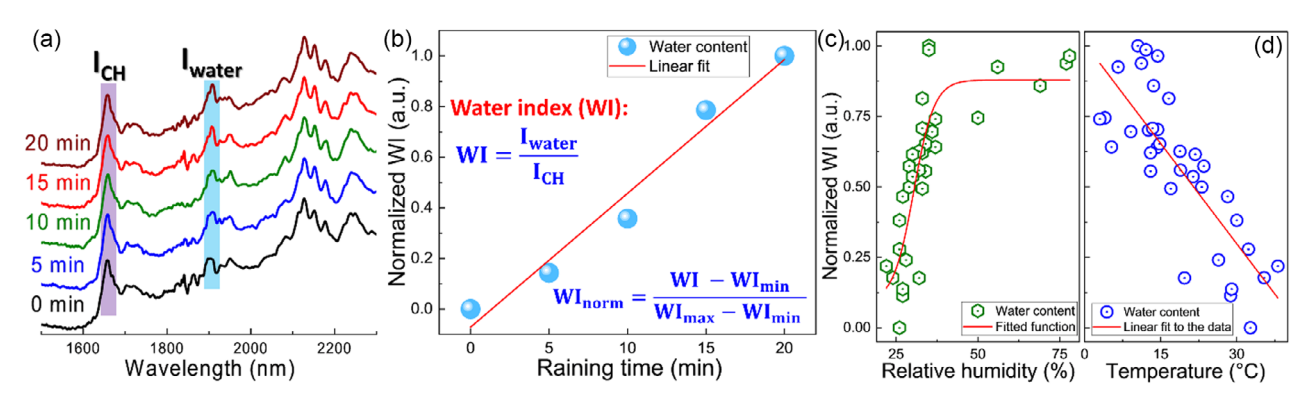


FIGURE 1 | Short-term NIR monitoring of water uptake in PV module BS (a, b) evolution of the NIRA spectrum (a) and WI index (b) of exemplary BS during rain exposure, (c) relationship between WI and RH, and (d) ambient temperature for rooftop-monitored modules.

comparison between modules with different absolute absorbance values and reduces baseline bias caused by BS thickness, surface roughness, or sensor positioning (Figure 1b).

The normalized WI is plotted in Figure 1b as a function of duration of rain exposure, with measurements recorded after 5, 10, and 20 min. A clear linear increase in the WI is observed over the 20-minute interval, indicating a consistent rise in NIR-detectable water content throughout the measurement period. A linear fit to the data yielded a coefficient of determination of  $R^2 = 0.98$ , confirming the strong correlation with time.

A long-term monitoring study was carried out on a PV module (FC/PET/PP, where FC is fluorinated coating and PP is polypropylene) installed at the HIERN rooftop testing facility. The module was equipped with temperature and RH sensors on the BS surface, and NIR measurements of the BS surface were performed daily from January to June 2024. The resulting WI data were analyzed in correlation with the recorded environmental parameters.

Figure 1c displays the dependence of the WI on RH. Two distinct regions can be observed: in the RH range of 20-45%, the WI increases approximately linearly from ~0.2 to 0.35. Above ~45% RH, the curve flattens, with the index reaching a plateau around 0.38-0.4, suggesting a saturation behavior. The plateau value reflects the maximum water retention capacity of the polymer under the given environmental conditions. While the measurements in Figure 1c were performed on a module with an FC-based BS, we have observed in separate campaigns (see Section 2.2) that plateau levels vary by material: PA and PET-based BSs tend to reach higher WI values, most probably due to their higher polarity and water sorption affinity, whereas fluorinated laminates typically show lower saturation levels, reflecting differences in the chemical structure, polarity, and microstructure (e.g., crystallinity and porosity) of the polymer layers. This behavior aligns with sorption isotherms commonly described by Langmuir-type models, where initial uptake occurs through physisorption on available polar sites, followed by pore or interlamellar saturation limiting further absorption [28, 29]. In contrast, Figure 1d shows an inverse correlation between temperature and the WI. Over the 5-month monitoring period, the water content decreases nearly linearly approximately from 0.4 at 0°C (winter) to 0.2 at 40°C (summer). Although RH often increases with ambient temperature under typical outdoor conditions, its relationship with temperature is nonlinear and influenced by varying vapor pressure and air moisture capacity. The observed saturation threshold and inverse trends with temperature suggest that both capillary condensation and reversible swelling of the polymer matrix contribute to the overall moisture dynamics [30–33].

# 2.2 | High-Throughput Spectral Mapping of Water Ingress in PV Modules

To evaluate water content distribution in PV modules with different BS types, near-infrared measurements were conducted on field-exposed modules at several PV plants in Northern Germany. Two measurement campaigns were performed in 2021 and 2023, enabling a comparative analysis over a 2-year interval. The measurements were conducted directly on-site from the BS side using a handheld NIR spectrometer.

Figure 2a displays WI histograms for three representative BS types—PA, FC, and PVDF—measured during the 2021 and 2023 campaigns under comparable weather conditions (Table 1). For all materials, a consistent shift toward higher WI values was observed in 2023 as compared to 2021, suggesting progressive moisture ingress during outdoor exposure. The magnitude and distribution of the shift vary by material. Although minor differences in recent weather conditions cannot be excluded, the consistent increase across all BS types supports the conclusion of progressive water ingress under long-term field exposure.

PA exhibits the most pronounced change, with the mean WI  $(\overline{W})$  increasing from 0.062 in 2021–0.082 in 2023. Additionally, the broad distribution in both years, as indicated by the large full width at half maximum (FWHM), reflects high variability in water ingress among the tested modules, which may be attributed to localized degradation effects or heterogeneity in field conditions. FC BSs also demonstrate an increase in  $\overline{W}$  from 0.082 to 0.108, though with a narrow distribution (FWHM: 0.018–0.022), indicating a more uniform water ingress. In contrast, PVDF BSs show the smallest increase in  $\overline{W}$ , rising from 0.070 to 0.082, and display a sharp narrowing of the FWHM from 0.018 to 0.008, implying both minimal ingress and consistent moisture resistance across modules. These trends underscore the material-dependent evolution of water ingress over time and highlight the stabilizing influence of fluorinated polymer layers [5, 34–37].

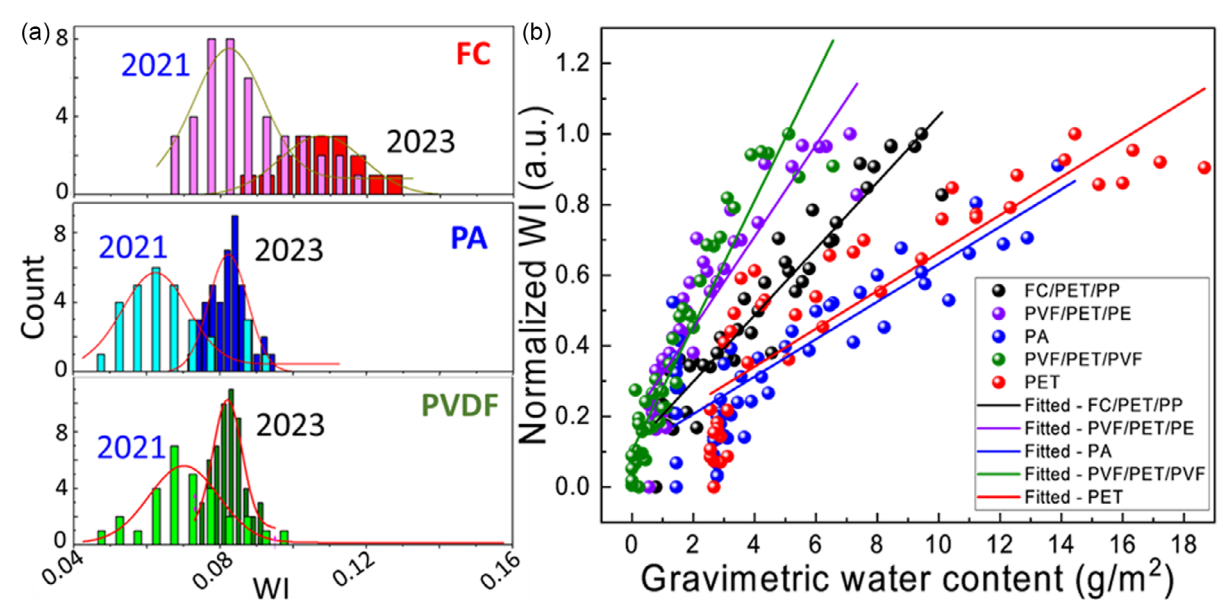


FIGURE 2 | Field and laboratory evaluation of long-term water ingress in PV modules with different BSs. (a) WI histograms for three BS types (PA, FC, PVDF) from 2021 and 2023 in Northern Germany. (b) Correlation between WI and gravimetric water content for BS samples.

**TABLE 1** | Mean water index and FWHM for different BS in 2021 and 2023.

	2021		2023	
Backsheet	Mean WI $[\overline{W}]$	FWHM	$W_{\mathrm{av}}$	FWHM
FC	0.082	0.018	0.108	0.022
PA	0.062	0.017	0.082	0.010
PVDF	0.070	0.018	0.082	0.008

Accurate quantification of moisture in PV module BSs requires not only relative indicators like the WI, but also absolute water content expressed as mass per area, a metric often requested by PV system operators. Additionally, since NIR spectral features of absorbed water vary with the chemical composition and structure of the polymer layers, material-specific calibration is necessary to ensure reliability across different BS types. To support the analysis of WI distributions observed in the field, a calibration dataset was generated under controlled laboratory conditions. Field-aged samples  $(3 \times 3 \text{ cm}^2)$  with various BS types—FC/ PET/PP, PVF/PET/PE, PA, PET, and DF (PVF/PET/PVF)—were exposed to moisture and subsequently dried while both mass loss and NIR spectra were recorded. Gravimetric water content (g m<sup>-2</sup>) was determined from the weight difference of BS samples before and after moisture exposure. Corresponding WI values were extracted from NIR absorbance near 1920 nm. To evaluate the relationship between absolute water uptake and the spectroscopically derived WI, gravimetric and NIR data were compared for various BS materials. WI values were min-max normalized independently for each material to account for differences in optical baseline and signal scaling, while gravimetric water content was retained in absolute units (g m<sup>-2</sup>) to preserve the physical comparability of moisture retention capacity. As shown in Figure 2b, the correlation between WI and water content varies significantly across different BS types. PA and PET-based BSs exhibited the highest overall water uptake, reaching values up

to 15-18 g m<sup>-2</sup>, with normalized WI values approaching saturation. In contrast, fluorinated laminates, such as FC/PET/PP and PVF/PET/PVF, absorbed considerably less water, typically below 7 g/m<sup>2</sup>, yet showed a substantial increase in WI. This divergence is further quantified by the slopes of the linear fits: PVF/PET/ PVF and PVF/PET/PE displayed the steepest slopes,  $0.177 \pm$  $0.009 \text{ g}^{-1} \text{ m}^2$  and  $0.130 \pm 0.009 \text{ g}^{-1} \text{ m}^2$ , respectively, followed by FC/PET/PP at  $0.094 \pm 0.004$ . The lowest slopes were observed for PET  $(0.054 \pm 0.004)$  and PA  $(0.053 \pm 0.005)$ , despite their higher water uptake. We hypothesize that these slope differences reflect not only the absolute moisture content, but also how water is distributed and interacts within the polymer matrix. Fluorinated laminates typically restrict moisture ingress to near-surface layers due to their low polarity and dense microstructure, resulting in a sharp spectral response even at low water content. As such, the WI increases rapidly with small changes in moisture load, likely due to surface accumulation or interfacial localization of water molecules. This is consistent with previous reports showing enhanced early-stage spectroscopic signals in PVF-based and fluorinated BSs due to their limited permeability and strong O-H dipole interactions [16, 34]. Conversely, hygroscopic polymers, such as PA and PET, exhibit bulk diffusion behavior, where water is absorbed deeply and homogeneously throughout the material volume. Although this results in a higher overall uptake, the NIR-active O-H overtones around 1920 nm originate primarily from near-surface light-matter interactions. As a result, the apparent WI grows more slowly as water becomes diluted across the matrix, and local concentration gradients are flattened. These assumptions are supported by the reported studies on PA and PET BSs showing high diffusion coefficients and moisture-buffering behavior under field or accelerated aging conditions [4, 6]. Altogether, the combined gravimetric and spectral analysis highlights the importance of both total water uptake and its spatial distribution in determining the NIR spectroscopic response. The observed slope trends confirm that the sensitivity and diagnostic value of WI are highly material-specific.

# 2.3 | Spatial Mapping of Water Ingress in PV Modules: From Momentary to Continuous Monitoring at the Module Level

Spatially resolved water mapping enables the detection of localized moisture accumulation and potential ingress pathways, including delaminated areas, loose interfaces, and cracks in either the glass or the BS. The mapping provides insights into how and where water enters the module, supporting more accurate diagnostics and improving reliability assessments. Grid-wise spectral measurements can be used to plot spatial maps of water distribution in PV polymers, helping identify sections most vulnerable to water ingress and providing insights into degradation mechanisms under field exposure. Accordingly, two regimes were tested: (i) water mapping in the BS of a module with partially delaminated packaging plotted by backside measurements, and (ii) water mapping in EVA encapsulants plotted using frontal measurements through the glass. In the latter case, we also demonstrated the feasibility of continuous monitoring and mapping of water ingress for a series of PV modules kept in prolonged contact with water.

A partially delaminated PV module exhibiting visible polymer separation (a "water pocket") was selected to visualize localized moisture ingress into the BS under real-world conditions. Measurements were performed 30 min after rainfall using a 60-point grid on the back side of a PV module, without any interruption of its performance. The resulting spatial WI distribution is shown in Figure 3a, with a photograph of the defect area highlighting the delaminated zone. A clear local maximum (WI  $\approx 1.0$ ) is observed at the delaminated site, while surrounding regions show elevated WI values in the range of 0.4–0.5. This suggests that BS delamination facilitates water accumulation not only at the defect but also in adjacent regions, potentially allowing

moisture to access the electrical circuitry and accelerate further degradation [2, 38, 39].

Moisture distribution in EVA encapsulants was further investigated on two identical modules with FC BSs taken from the same batch: one field-aged outdoors for approximately 10 years, and one stored under sheltered conditions for the same period. Both modules were mapped from the frontal side using a handheld near-infrared spectrometer, taking advantage of the unique ability of NIRA to probe polymer layers through the front glass. A measurement grid of  $11 \times 9$  points covered ~24 solar cells per module, including active areas, intercell gaps, and busbars. An exemplary WI map is shown in Figure 3c, revealing nonuniform spatial distributions.

Both modules were then immersed in an aqueous electrolyte and monitored over 31 days to track the kinetics of moisture ingress. Time-resolved WI maps are presented in Figure 3b, showing how moisture penetrated into the encapsulant. Initially (day 0), WI values were low (~0.06-0.08), especially at cell centers. By day 1, increased uptake was apparent and more pronounced in the field-aged module. By day 8, water accumulation was visible in both modules, particularly between cells. From day 9 to day 31, saturation progressed. The stored module showed a relatively even distribution of WI, while the field-aged module developed localized saturation zones near the center of the mapped area. In both cases, intercell regions consistently exhibited higher WI than cell centers, indicating that water primarily entered through the BS rather than from the edges or module perimeter. This could be due to the module structure in the areas between cells, the encapsulant (EVA) is present on both sides without interruption by a silicon cell, potentially leading to higher moisture accumulation.

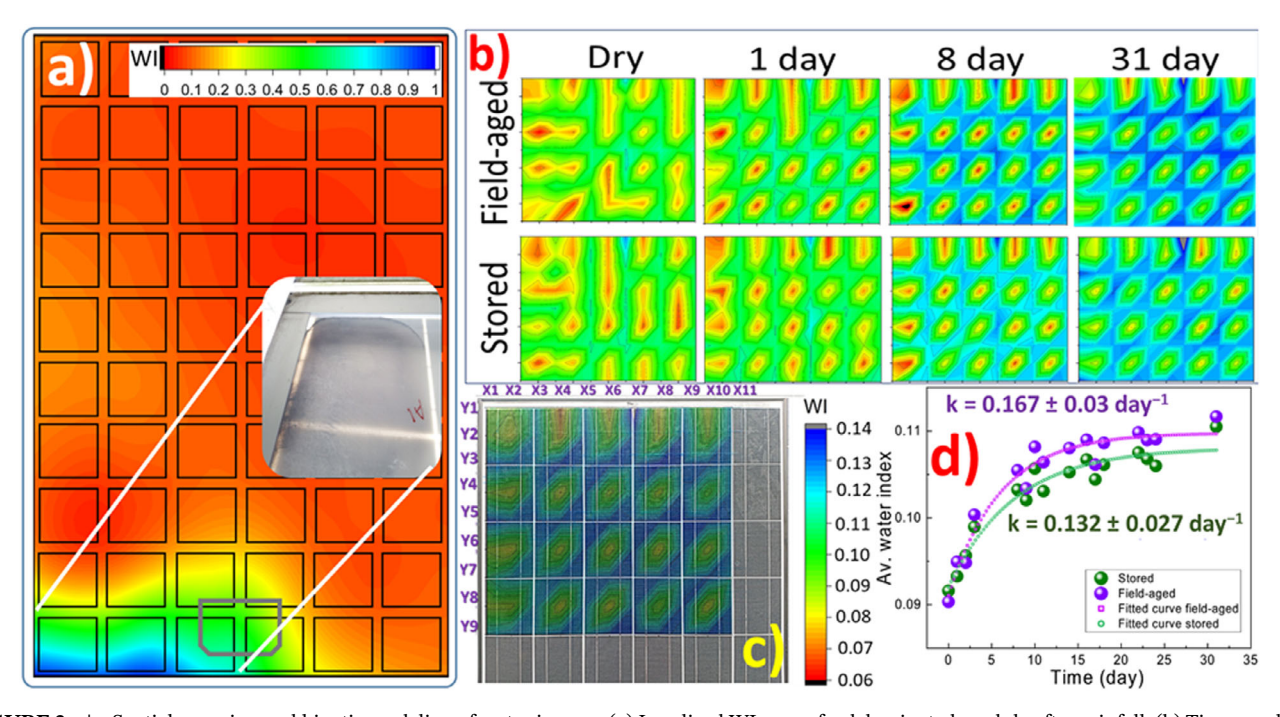


FIGURE 3 | Spatial mapping and kinetic modeling of water ingress. (a) Localized WI map of a delaminated module after rainfall. (b) Time-resolved WI evolution during 31-day immersion for two FC-based modules. (c) Example 2D WI map overlapped with a photograph of the tested module showing spatial variation of WI. (d) Time-dependent water uptake curves for two tested PV modules.

Kinetic modeling of the average WI (Figure 3d) was performed using a time-dependent exponential saturation function derived from Langmuir adsorption theory. The Langmuir kinetic model describes a first-order sorption process in systems with a finite number of adsorption sites, where the uptake rate decreases as sites become progressively occupied [40–43].

The time-dependent change in the WI W(t) was modeled using the following expression:

$$W(t) = A \cdot \left(1 - e^{-kt}\right) + C \tag{1}$$

where A is the amplitude of water uptake above the baseline level C, C is the initial WI, and k is the apparent sorption rate constant.

The model captures the saturation-limited nature of water ingress in polymeric BSs and encapsulants. The fitted rate constants revealed distinct differences between the two modules: the field-aged module exhibited a higher sorption rate constant of  $0.167 \pm 0.03 \, \mathrm{day}^{-1}$ , while the stored module showed a slower uptake with a rate constant of  $0.132 \pm 0.027 \, \mathrm{day}^{-1}$ . The resulting curves closely matched the experimental data across 31 days of immersion, with model performance yielding  $R^2 = 0.95$  and RMSE = 0.00133 for the field-aged module, and  $R^2 = 0.94$ , RMSE = 0.00124 for the stored module. These results indicate that the Langmuir-type first-order kinetic model adequately describes the observed moisture uptake behavior in PV modules subjected to different exposure histories.

# 3 | Conclusion

NIRA spectroscopy was applied to monitor and quantify moisture ingress in PV modules by analyzing the intensity of the 1910-1920 nm water-related absorption band. A WI derived from this band enabled nondestructive assessment of water uptake under realistic exposure conditions and across multiple degradation scenarios. Short-term field measurements during rainfall revealed a 14% increase in the WI within 20 min, indicating rapid moisture ingress into encapsulants and BSs. Continuous rooftop monitoring over 5 months showed strong environmental correlations: the index increased by approximately 75% as RH rose from 20% to 50%, and decreased by 50% as ambient temperature rose from 0°C to 40°C. Comparative field measurements from 2021 and 2023 enabled analysis of moisture accumulation trends across different BS materials. While different module sets were used in each campaign, all measurements were conducted under comparable ambient conditions and identical protocols. The WI increased by ~32% for PA and FC-coated BSs, and by ~17% for PVDF. The spread of WI values increased by 70% for PA and 22% for FC-coated BSs, while narrowing by 56% for PVDF, indicating material-dependent degradation variability. Lab gravimetric measurements on field-aged samples confirmed corresponding water uptake ranging from <0.4 g m<sup>-2</sup> for fluorinated laminates to ~0.9 g m<sup>-2</sup> for PA and PET-based structures. Spatially resolved near-infrared mapping of a field-aged module with visible BS damage revealed localized increases in the normalized WI, with delaminated areas reaching the maximum observed value ( $\sim$ 1.0), while surrounding regions exhibited values around 0.4-0.5. Long-term immersion experiments on two structurally identical fluoropolymer-coated modules-one field-aged, one

stored—demonstrated increased uptake in the aged sample. The sorption rate constants derived from Langmuir-type kinetic fits were  $0.167 \pm 0.03$  and  $0.132 \pm 0.027$  day<sup>-1</sup>, respectively, corresponding to a 26.5% faster uptake in the aged module (R<sup>2</sup> = 0.95 and 0.94; RMSE < 0.0014 for both).

The study introduces near-infrared spectroscopy as a reliable, versatile, and noninvasive approach to quantifying moisture uptake in PV modules with material specificity and temporal resolution. Its ability to detect both gradual changes under environmental exposure and localized anomalies enables targeted analysis of degradation patterns. These findings establish NIRA as a valuable diagnostic tool for evaluating PV reliability and degradation in the field.

## 4 | Experimental Section

Spectral Instruments. High-resolution NIRA spectra were acquired using a fiber-coupled FT-NIR Rocket L1-025-2TE spectrometer (ARCoptix, Switzerland), operating in the spectral range of 900-2500 nm (4000-11100 cm<sup>-1</sup>) with a spectral resolution of 2 cm<sup>-1</sup>. Samples were illuminated using a stabilized fiber-coupled NIR light source, SLS201/M (Thorlabs, Germany). Both the NIR lamp and the spectrometer were linked via optical fibers (M35L. 400–2200 nm, fiber core diameter of 1000μm, Thorlabs, Germany) to an RPH-SMA probe block (Thorlabs, Germany). The incoming and outgoing light beams formed a 90° angle. The probe was positioned on the sample surface and manually held during measurements. The diameter of the light spot on the sample surface was approximately 2 mm, shielded from ambient light by the measuring head, ensuring no interference from solar or indoor illumination. As a standard practice, 20 consecutive reflectance spectra were acquired (with each spectrum taking approximately 1s to capture) and subsequently averaged to reduce noise. Measurements were typically performed on the rear (air-facing) side of PV modules behind a Si solar cell to avoid the intrusion of solar irradiation into the detection system.

The NIRONE S2.0/S2.2 (Spectral Engines, Finland) is a portable, lightweight device that utilizes a micro-electro-mechanical system (MEMS) Fabry-Perot Interferometer coupled with a single InGaAs photodetector. It features a fully programmable optical filter with a spectral range from 1550 to 1950 nm (S2.0) and from 1750 to 2150 nm (S2.2), and a spectral acquisition step of 10 nm. The NIRONE sensor, covered with a custom-made polyurethane protective housing, was positioned on the surface of the BS beneath the silicon cell and manually held in place during measurements. Similar to the probe used with the ArcOptix device, the sensor itself shields the inspected spot (ca. 1 cm²) from solar light ingress. At the start of the measurement process, the sensors were calibrated by recording reference spectra in the dark and from an illuminated Spectrolon standard. The typical acquisition time was set to 50 ms.

Analysis of Spectra. NIRA spectra of BSs and EVA encapsulants were processed using a customized Python script performing automated spectral preprocessing (cutting and baseline correction), BS type identification, and calculation of water indices. BS types were determined by evaluating the ratio of NIRA peak intensities at 1660 and 1730 nm, corresponding to =C-H and

-C-H stretching vibrations in PET and other BS constituents, as described in previous studies [18, 44]. The WI was computed as the ratio of the integrated absorbance of the water-related band centered at 1910 nm (integration range: 1880–1920 nm) to the reference -C-H band at 1730 nm. This range was selected to maximize signal stability and minimize noise and overlapping polymer signals in both benchtop and portable NIR setups [22].

#### Acknowledgments

All authors contributed equally to this work. This work is supported by the German Federal Ministry for Economic Affairs and Climate Action ("dig4morE", Number 03EE1090B, "REMBup" FKZ 03EWR021F), the Helmholtz Association in the framework of the innovation platform "Solar TAP" (Number 714-62150-3/1 (2023)). However, the views and opinions expressed are solely those of the authors and do not necessarily reflect those of the European Union or the European Research Council. Neither the European Union nor the granting authority can be held responsible for them.

Open Access funding enabled and organized by Projekt DEAL.

#### **Conflicts of Interest**

The authors declare no conflicts of interest.

#### **Data Availability Statement**

The data supporting the findings of this study are available from the corresponding author upon reasonable request.

#### References

- 1. N. Ketjoy, P. Mensin, and W. Chamsa-Ard, "Impacts on Insulation Resistance of Thin Film Modules: A Case Study of a Flooding of a Photovoltaic Power Plant in Thailand," *PloS One* 17 (2022): e0274839.
- 2. O. K. Segbefia, N. Akhtar, and T. O. Sætre, "Moisture Induced Degradation in Field-Aged Multicrystalline Silicon Photovoltaic Modules,: *Solar Energy Materials and Solar Cells* 528 (2023): 112407.
- 3. O. K. Segbefia, A. G. Imenes, and T. O. Sætre, "Moisture Ingress in Photovoltaic Modules: A Review," *Solar Energy* 224 (2021): 889–906.
- 4. Y. Lyu, A. Fairbrother, M. Gong, et al., "Drivers for the Cracking of Multilayer Polyamide-Based Backsheets in Field Photovoltaic Modules: In-Depth Degradation Mapping Analysis," *Progress in Photovoltaics: Research and Applications* 28 (2020): 704–716.
- 5. J. Pascual, M. García, J. Marcos, and L. Marroyo, "Analysis of Polyamide and Fluoropolymer Backsheets: Degradation and Insulation Failure in Field-Aged Photovoltaic Modules," *Progress in Photovoltaics: Research and Applications* 31 (2023): 494–505.
- 6. A. Omazic, G. Oreski, M. Halwachs, et al., "Relation between Degradation of Polymeric Components in Crystalline Silicon PV Module and Climatic Conditions: A Literature Review," *Solar Energy Materials and Solar Cells* 192 (2019); 123–133.
- 7. A. Sinha, S. Roy, S. Kumar, and R. Gupta, "Investigation of Degradation in Photovoltaic Modules by Infrared and Electroluminescence Imaging," in *Advances in Optical Science and Engineering: Proceedings of the Third International Conference, OPTRONIX* (Springer, 2016), 3–9.
- 8. L. Neumaier, G. C. Eder, Y. Voronko, K. A. Berger, G. Újvári, and K. Knöbl, "Advanced UV-Fluorescence Image Analysis for Early Detection of PV-Power Degradation," *EPJ Photovoltaics* 14 (2023):9.
- 9. C. Buerhop-Lutz, O. Stroyuk, O. Mashkov, J. A. Hauch, and I. M. Peters, "Unveiling the Potential of Ultraviolet Fluorescence Imaging as a Versatile Inspection Tool: Insights From Extensive

- Photovoltaic Module Inspections in Multi-MWp Photovoltaic Power Stations," *Solar RRL* 8 no. 24 (2024): 2400566, https://doi.org/10.1002/solr.202400566.
- 10. M. Köntges, S. Kurtz,, C. E. Packard, et al., Review of Failures of Photovoltaic Modules (IEA-PVPS, 2014).
- 11. X. Wu, J. Li, L. Yao, and Z. Xu, "Auto-Sorting Commonly Recovered Plastics From Waste Household Appliances and Electronics Using Near-Infrared Spectroscopy," *Journal of Cleaner Production* 246 (2020): 118732.
- 12. E. Aronson and P. Waldén, "Using Near-Infrared Spectroscopy for Characterization of Transiting Exoplanets," *Astronomy & Astrophysics* 578 (2015): A133.
- 13. M. Jamrógiewicz, "Application of the Near-Infrared Spectroscopy in the Pharmaceutical Technology," *Journal of Pharmaceutical and Biomedical Analysis* 66 (2012): 1–10.
- 14. A. Sakudo, "Near-Infrared Spectroscopy for Medical Applications: Current Status and Future Perspectives," *Clinica Chimica Acta* 455 (2016): 181–188.
- 15. Y. Wang, C. Zhao, H. Tian, et al., "NIRS-Based Detection Advances in Agriculture: Data Enhancement, Characteristic Wavelength Selection and Modelling Techniques," *Spectrochimica Acta Part A: Molecular and Biomolecular Spectroscopy* 343 (2025): 126611.
- 16. C. Barretta, G. Oreski, S. Feldbacher, K. Resch-Fauster, and R. Pantani, "Comparison of Degradation Behavior of Newly Developed Encapsulation Materials for Photovoltaic Applications under Different Artificial Ageing Tests," *Polymers* 13 (2021): 271.
- 17. K. B. Beć and C. W. Huck, "Breakthrough Potential in Near-Infrared Spectroscopy Spectra Simulation. A Review of Recent Developments," *Frontiers in Chemistry* 7 (2019): 48, https://doi.org/10.3389/fchem.2019. 00048.
- 18. O. Stroyuk, C. Buerhop-Lutz, A. Vetter, J. Hauch, and C. J. Brabec, "Nondestructive Characterization of Polymeric Components of Silicon Solar Modules by Near-Infrared Absorption Spectroscopy (NIRA)," *Solar Energy Materials and Solar Cells* 216 (2020): 110702.
- 19. G. Gullifa, L. Barone, E. Papa, A. Giuffrida, S. Materazzi, and R. Risoluti, "Portable NIR Spectroscopy: The Route to Green Analytical Chemistry," *Frontiers in Chemistry* 11 (2023): 1214825, https://doi.org/10.3389/fchem.2023.1214825.
- 20. J. Markert, S. Kotterer, D. E. Mansour, D. Philipp, and P. Gebhardt, "Advanced Analysis of Backsheet Failures From 26 Power Plants," *EPJ Photovoltaics* 12 (2021): 7.
- 21. C. Buerhop-Lutz, O. Stroyuk, T. Pickel, T. Winkler, J. Hauch, and I. M. Peters, "PV Modules and Their Backsheets A Case Study of a Multi-MW PV Power Station," *Solar Energy Materials and Solar Cells* 231 (2021): 111295.
- 22. O. Stroyuk, C. Buerhop, E. Wittman, et al., "Assessing Field Degradation of Photovoltaic Modules by Near-Infrared Absorption Spectroscopy of Ethylene Vinyl Acetate Encapsulant," *Solar RRL* 8 no. 8 (2024): 2301022, https://doi.org/10.1002/solr.202301022.
- 23. A. R. Dusane, P. Lenarda, and M. Paggi, "Computational Modeling of Viscoelastic Backsheet Materials for Photovoltaics," *Mechanics of Materials* 186 (2023): 104810.
- 24. H. Li, R. Kikuchi, M. Kumagai, et al., "Nondestructive Estimation of Strength Deterioration in Photovoltaic Backsheets Using a Portable near Infrared Spectrometer," *Solar Energy Materials and Solar Cells* 101 (2012): 166–169,
- 25. R. Tsenkova, J. Munćan, B. Pollner, and Z. Kovacs, "Essentials of Aquaphotomics and Its Chemometrics Approaches," *Frontiers in Chemistry* 6 (2018): 363, https://doi.org/10.3389/fchem.2018.00363.
- 26. J. Sundaram, S. Mani, C. V. K. Kandala, and R.A. Holser, "Application of NIR Reflectance Spectroscopy on Rapid Determination of Moisture

- Content of Wood Pellets," American Journal of Analytical Chemistry 06 (2015): 923–932.
- 27. M. Manley, "Near-Infrared Spectroscopy and Hyperspectral Imaging: Non-Destructive Analysis of Biological Materials," *Chemical Society Reviews* 43 (2014): 8200–3214.
- 28. B. D. Freeman, "Basis of Permeability/Selectivity Tradeoff Relations in Polymeric Gas Separation Membranes," *Macromolecules* 32 (1999): 375–380.
- 29. K. C. Ng, M. Burhan, M. W. Shahzad, and A. B. Ismail, "A Universal Isotherm Model to Capture Adsorption Uptake and Energy Distribution of Porous Heterogeneous Surface," *Scientific Reports* 7 no. 1 (2017): 10634, https://doi.org/10.1038/s41598-017-11156-6.
- 30. B. L. Foley, S. Aubry, M. Murialdo, and E. A. Glascoe, "Rigorous Models for Vapor Diffusion in Polymers with Immobilization and Chemical Potential Gradients," *The Journal of Physical Chemistry B* 128 (2024): 9274–9283.
- 31. F. Deng, Z. Chen, C. Wang, C. Xiang, P. Poredoš, and R. Wang, "Hygroscopic Porous Polymer for Sorption-Based Atmospheric Water Harvesting," *Advanced Science* 9 no. 33 (2022): 2204724, https://doi.org/10.1002/advs.202204724.
- 32. M. Chen, B. Coasne, R. Guyer, D. Derome, and J. Carmeliet, "Role of Hydrogen Bonding in Hysteresis Observed in Sorption-Induced Swelling of Soft Nanoporous Polymers," *Nature Communications* 9 no. 1 (2018): 3507, https://doi.org/10.1038/s41467-018-05897-9.
- 33. A. Singh and M. Mukherjee, "Swelling Dynamics of Ultrathin Polymer Films," *Macromolecules* 36 (2003): 8728-8731.
- 34. C. Buerhop, O. Stroyuk, J. Zöcklein, T. Pickel, J. Hauch, and I. M. Peters, "I.M. 2022, Wet Leakage Resistance Development of Modules with Various Backsheet Types," *Progress in Photovoltaics: Research and Applications* 30 (2020): 938–947.
- 35. J.-W. Zhang, K. Feng, S. Diaham, Q.-Q. Liao, X. Zhou, and C. Putson, "Lifetime Evaluation of Photovoltaic Polymeric Backsheets under Ultraviolet Radiation: From Chemical Properties to Mechanical Modeling," *ACS Omega* 7 (2022): 45609–45616.
- 36. A. A. Abdallah, M. Abdelrahim, M. Elgaili, M. Pasha, K. Mroue, and A. Abutaha, "Degradation of Photovoltaic Module Backsheet Materials in Desert Climate," *Solar Energy Materials and Solar Cells* 277 (2024): 113118.
- 37. S. L. Moffitt, P.-C. Pan, L. Perry, et al., "Microstructure Changes during Failure of PVDF-Based Photovoltaic Backsheets," *Progress in Photovoltaics: Research and Applications* 31 (2023): 26–35.
- 38. M. Aghaei, A. Fairbrother, A. Gok, et al., "Review of Degradation and Failure Phenomena in Photovoltaic Modules," *J. Renewable and Sustainable Energy Reviews* 159 (2022): 112166.
- 39. J. Kim, M. Rabelo, S. P. Padi, H. Yousuf, E.-C. Cho, and J. Yi, "A Review of the Degradation of Photovoltaic Modules for Life Expectancy.," *Energies* 14 (2021): 4278.
- 40. Y. S. Ho and G. McKay, "Pseudo-Second Order Model for Sorption Processes," *Process Biochemistry* 34 (1999): 451–461.
- 41. A. R. Berens and H. B. Hopfenberg, "Diffusion and Relaxation in Glassy Polymer Powders: Separation of Diffusion and Relaxation Parameters.," *Polymer* 19 (1978): 489–496.
- 42. S. Mitterhofer, C. Barretta, L. F. Castillon, G. Oreski, M. Topič, and M. Jankovec, "A Dual-Transport Model of Moisture Diffusion in PV Encapsulants for Finite-Element Simulations," *IEEE Journal of Photovoltaics* 10 (2020): 94–102.
- 43. S. T. Castonguay, P. Roy, Y. Sun, et al., Modeling Diffusion and Types I-V Sorption of Water Vapor in Heterogeneous Systems," *H.N, Chemical Engineering Science* 275 (2023): 118695.
- 44. O. Stroyuk, C. Buerhop-Lutz, A. Vetter, et al., "Distinguishing between Different Types of Multi-Layered PET-Based Backsheets of

PV Modules with Near-Infrared Spectroscopy," *Progress in Photovoltaics: Research and Applications* 30 (2022): 859–868.